Infrared Physics and Technology 106 (2020) 103278

Contents lists available at ScienceDirect

Infrared Physics & Technology

journal homepage: www.elsevier.com/locate/infrared

Ultra-compact QEPAS acoustic detection module with acoustic wave confinement

Haoyang Lin[a], Zhao Huang[a], Yihua Liu[a], Ruifeng Kan[b], Huadan Zheng[a,c,*], Renjing Zhang[a], Wenguo Zhu[a,c], Jieyuan Tang[a,c], Jianhui Yu[a,c], Zhe Chen[a,c], Frank K Tittel[d]

[a] Key Laboratory of Optoelectronic Information and Sensing Technologies of Guangdong Higher Education Institutes, Department of Optoelectronic Engineering, Jinan University, Guangzhou 510632, China
[b] State Key Laboratory of Applied Optics, Changchun Institute of Optics, Fine Mechanics and Physics, Chinese Academy of Sciences, Changchun 130033, China
[c] Key Laboratory of Visible Light Communications of Guangzhou, Jinan University, Guangzhou 510632, China
[d] Department of Electrical and Computer Engineering, Rice University, Houston, TX 77005, USA

ARTICLE INFO

Keywords:
Photoacoustic spectroscopy
Quartz-enhanced photoacoustic
Quartz tuning fork
Spectroscopy
Trace gas detection

ABSTRACT

An ultra-compact acoustic detection module (ADM) was developed for trace gas detection by use of quartz-enhanced photoacoustic spectroscopy (QEPAS). Different from the conventional QEPAS ADM, a gas enclosure was employed to confine the photoacoustic waves and excite the acoustic azimuthal and radial modes. Finite element modelling (FEM) method was used to analyze the acoustic modes and pressure distribution. The geometrical parameters of the ADM were optimized to enhance the sensor performance. The developed QEPAS ADM was only ~0.05 mL and ~0.15 g, significantly reducing the QEPAS sensor volume and weight, and improving the QEPAS system gas flush time by orders of magnitude. As a proof of concept, H_2O was detected by the ultra-compact spectrophone employing a telecommunication diode laser. A detection limit of 2 ppm was achieved.

1. Introduction

Photoacoustic spectroscopy (PAS) is a practical approach for optical trace gas sensing with the advantages of high sensitivity, compact size, wide dynamic range and simplicity of use. The principle of PAS is detection of the acoustic waves generated by the target analytes upon the absorption of optical radiation [1,2]. An acoustic transducer to convert the acoustic signal into an electric signal is usually a microphone, a cantilever or a piezoelectric film. PAS has been successfully applied to applications including atmospheric pollution monitoring, agricultural and industrial processes control as well as medical diagnostics [3]. For example, PAS has been used for monitoring nitric oxide (NO) in vehicle exhaust emissions [4] and methane (CH_4) in atmospheric pollution [5].

As a variant of PAS, quartz-enhanced photoacoustic spectroscopy (QEPAS) has been booming developed in the past decades [3–6], since its invention by A. Kosterev in 2002 [7]. The innovation of QEPAS is using a sharply resonant quartz tuning fork (QTF), instead of a microphone, to accumulate acoustic energy by means of piezoelectric effect. The prominent features of QEPAS are an ultra-compact setup, low cost and high noise immunity [8–15]. The high noise immunity of QEPAS can be attributed to the anti-symmetric vibration, a high quality factor (Q factor) and the narrow resonant bandwidth of a QTF [16,17]. QTF can also be used as a thermal wave collector for light-induced thermoelastic spectroscopy (LITES), in which the QTF was driven to vibrate by the heat basing on the thermoelastic effect [18–20]. A commercially available QTF has a resonant frequency of 32.7 kHz and a high Q factor of $\sim 10^5$ in vacuum. The Q factor of QTF packaged in metal encapsulation was measured to be 7×10^4–8×10^4. The Q factors decrease to 8,000–10,000 in the atmosphere due to the air damping.

Acoustic detection module (ADM), consisting of a QTF and a gas enclosure, is the core of the QEPAS system [21]. The construction of the ADMs determined the QEPAS sensor performance and their applications. The first generation of ADM reported by our previous publication [22] was based on KF25 vacuum components. The gas enclosure was made of a KF25 vacuum flange with a diameter of 22.5 mm and a height of 20.6 mm, corresponding to a volume of 8,186.6 mm^3. A KF25 vacuum feedthrough flange was used as the base of the gas enclosure to transfer the electrical signals of the QTF. The second generation of ADM was designed as a cubic shape with the dimension was 25 mm × 25 mm × 15 mm, corresponding to a volume of 9,375 mm^3 [9]. In the second generation of ADM, the KF25 vacuum feedthrough was removed, making the ADM more portable. Fiber-coupled ADM was

* Corresponding author at: Key Laboratory of Optoelectronic Information and Sensing Technologies of Guangdong Higher Education Institutes, Department of Optoelectronic Engineering, Jinan University, Guangzhou 510632, China.
E-mail address: zhenghuadan@jnu.edu.cn (H. Zheng).

https://doi.org/10.1016/j.infrared.2020.103278
Received 23 December 2019; Received in revised form 14 March 2020; Accepted 15 March 2020
Available online 20 March 2020
1350-4495/

developed for industrial application by mounting the QTF and the optical fiber focuser together using a telecom-style butterfly packaging. The fiber-coupled ADM has a rectangular shape with the dimensions of 20 mm × 12.7 mm × 8.5 mm, corresponding to a volume of 2,159 mm^3 [23]. Recently, custom tuning forks with low resonant frequencies and high *Q* factors were demonstrated by Spagnolo, which benefits the collimation of laser beam and detection of molecules with fast vibration to translation relaxation rate [24–27]. The ADM for the custom tuning forks has a cuboid main body with the dimensions of 57 mm × 57 mm × 35 mm, corresponding to a volume of 113,715 mm^3 [28]. A 3D printing technique was introduced to a QEPAS sensor to fabricate a 3D-printed ADM and compress its volume. The compressed ADM still shows a length of 29 mm and a width of 15 mm [29].

In this paper, we demonstrate the most compact QEPAS ADM ever, to the best of our knowledge. The volume of the developed ADM was comparable to the enclosed standard QTF, significantly reducing the QEPAS sensor size and providing orders of magnitude shorter ADM gas flush time. The effect of the acoustic wave confinement in the ADM was simulated by the finite element modelling (FEM) method. The geometry of the ADM was optimized to obtain better sensor performance. The long-term stability of the ultra-compact QEPAS ADM was evaluated.

2. Fabrication of the ultra-compact QEPAS ADM

In QEPAS, an ADM is the key component which determines the performance of the sensor. In the fabrication of conventional QEPAS ADM, one-dimensional acoustic resonators made of a narrow tube with two open ends are assembled with the QTF to confine the acoustic waves, forming a spectrophone. Then a gas enclosure is used to separate the spectrophone from the surroundings, forming an ADM. In this work, a gas enclosure was designed as a spectrophone forming an ultra-compact ADM. The schematic diagram of the ultra-compact ADM was shown in Fig. 1. The ADM is designed as a cylindrical cavity to confine the acoustic azimuthal and radial modes. Two planiform windows were fabricated symmetrically on the ADM wall. Since the diameter of the widow is < 1 mm, the small gap between the cylinder cell and the window can be sealed by soft epoxy resin to guarantee the gas tightness

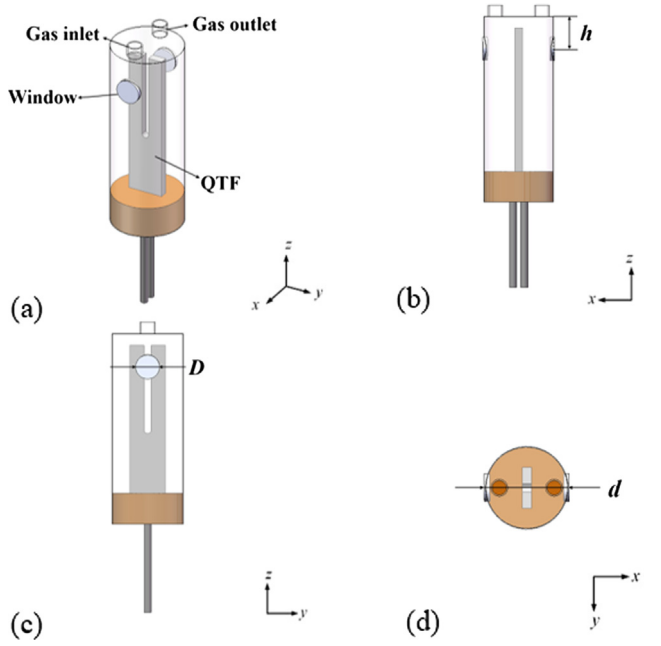

Fig. 1. Schematic diagram of the developed ultra-compact QEPAS ADM. *R*:ADM radius; *D*: window diameter, *h*: distance between the window and ADM top; *d*: ADM length.

of the ADM. The distance between the ADM top and the window center of ~ 1.4 mm, where corresponds a 0.7 mm from the QTF top to the window center, is the optimum position to accommodate the laser beam. The laser with a beam waist of 0.1 mm goes through the QTF gap from the window. The ADM wall thickness was designed to be 0.18 mm. Two holes connected with gas pipe were set on the top of the ADM for gas inlet and gas outlet. The overall size of the ultra-compact ADM is comparable with a commercially available 32768 Hz QTF with a dual in-line pin package. The volume and weight of the ADM were ~ 0.05 mL and 0.15 g, respectively.

The resonance frequencies f_{jmq} of the ADM can be expressed as follows:

$$f_{jmq} = \frac{c}{2}\sqrt{\left(\left(\frac{a_{jm}}{R}\right)^2\left(\frac{q}{d}\right)^2\right)} \quad (1)$$

where *R* and *d* are the radius and length of the ADM, *j*, *m*, *q* are the eigenvalues of the radial, azimuthal, and longitudinal modes respectively, and a_{jm} is the j_{th} zero of the derivative of the m_{th} Bessel function divided by π.

3. Experimental setup

A typical QEPAS experimental setup was depicted in Fig. 2. After checking the lasers in stock, a 1.39 μm near-infrared fiber coupled distributed feedback (DFB) diode laser was employed for H_2O detection as a proof of concept. A custom control electronic unit (CEU) as reported in our previous publication [10] was employed as the laser driver to control the temperature and injection current of the diode laser. 2*f* wavelength modulation technique was used to increase the QEPAS detection sensitivity. A ramp signal with a frequency of 10 mHz and a sine signal with a frequency of $f_0/2$, where f_0 is the resonance frequency of the QTF, were added to the laser driver. The 2*f* harmonic wavelength modulation was used to minimize the background caused by stray radiation and also minimize the impact of spectral wings of interfering strong absorption lines [30]. The laser beam was focused through the ADM by means of a grin lens. The focal length of the grin lens was ~ 1 cm and the diameter of the beam waist was ~ 100 μm. The QTF output electrical signal is amplified by a custom transimpedance preamplifier with a 10 MΩ feedback resistor. A lock-in amplifier (Standford SR830) was used to demodulate the signal in a 2*f* mode. A LabView program displays the calculated H_2O vapor concentrations on a personal computer.

4. Optimization of QEPAS ADM

4.1. ADM length (Optical length)

The geometry of the QEPAS ADM was optimized to improve QEPAS performance. Along the laser beam axis, the radius *R* was larger than length *d*, thus the acoustic azimuthal and radial modes dominates in the ADM. The acoustic pressure variation in QEPAS ADM was analyzed by FEM method using COMSOL Multiphysics®. The QTF prong width, thickness and spacing were set as 600 μm, 330 μm and 300 μm respectively. With the ADM perimeter fixed, the length was set as 2.8 mm, 2.6 mm and 2 mm, respectively. The window diameter *D* was set to 0.75 mm. The frequency of the acoustic waves was set to 32.7 kHz, referring to the QTF. In the simulation, acoustic wave's attenuation on the QTF prong surface and ADM inner wall was assumed to be zero. As shown in Fig. 3, when the ADM length *d* decreased to 2 mm, the acoustic pressure in the QTF prong spacing increased significantly.

In the experiment, the ADM length *d* was changed from 2.82 mm to 2 mm to evaluate the QEPAS signal. The obtained QEPAS 2*f* signal amplitude as a function of was plotted in Fig. 4. With the *d* decreased from 2.82 mm to 2 mm, the QEPAS signal amplitude increased by 73%, from 0.458 mV to 0.792 mV. The increase in signal amplitude can be

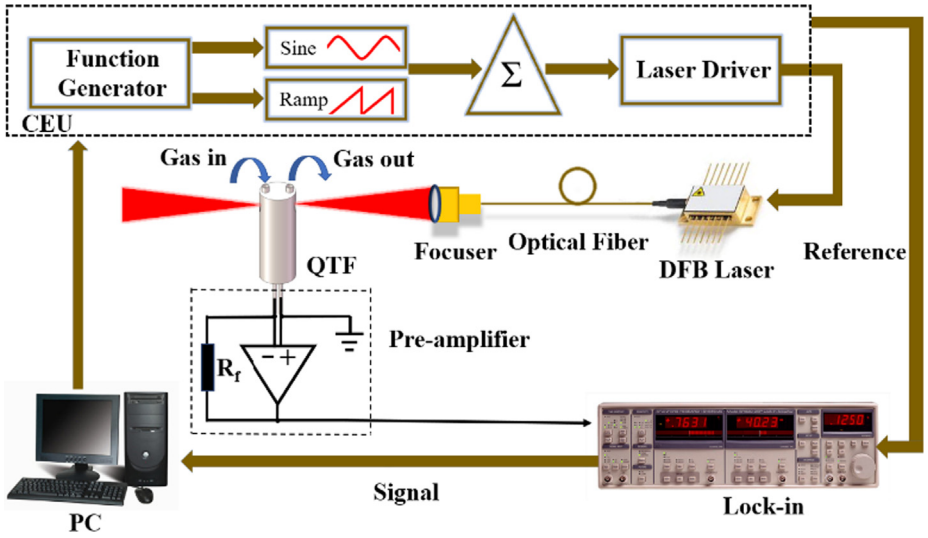

Fig. 2. QEPAS experimental setup. CEU: control electronic unit; Σ: adder; QTF: quartz tuning fork; DFB: distributed feedback laser; Lock-in: lock-in amplifier; R_f: feedback resistance; PC: personal computer.

attributed to the acoustic wave confined pressure increasement in both azimuthal and radial direction. The obtained results coincide well with the theoretical analysis.

4.2. Optimization of window diameters

The acoustic wave generated by the photoacoustic effects was confined by the cylindrical ADM. Two windows were fabricated on the wall of the ADM to accommodate the laser beam. Due to the different acoustic reflection coefficients between the ADM walls and windows, the acoustic modes in the ADM was affected. The gas sensor performance based on four ultra-compact QEPAS ADMs were evaluated, taking H_2O as proof of concept. Fig. 5. depicts the comparison of the 2*f* signals. A bare QTF acted as a reference. The H_2O concentration was controlled at 1.8%, as our previous experiment [31]. The laser temperature was set to 17.5 °C. The injection current was changed from 15 mA to 60 mA, corresponding to the emission wavelength from 7196 cm^{-1} to 7194.5 cm^{-1}. An H_2O absorption line located at 7194.8 cm^{-1} with an intensity of 3.07 × 10^{-21} cm/mol was targeted, according to the HITRAN database [32]. With the increasing of the window diameter *D*, the 2*f* signal amplitudes increased dramatically.

The performance of sensors based on four ADMs and a bare QTF were analyzed in Table 1. Due to the acoustic coupling effects between the QTF and the ADM, the resonance frequencies of the ADM varied by 3 Hz. The *Q* factors of the ADMs are slightly lower than the bare QTF due to the acoustic coupling effects. For sensors based on ADM#1, #2, #3 and bare QTF, the signal amplitudes were 4.95 × 10^{-4} V, 7.92 × 10^{-4} V, 8.48 × 10^{-4} V and 4.57 × 10^{-4} V, respectively. Compared to the bare QTF, the signal amplitudes obtained by the ADM#1, #2, #3 increased by 8%, 73% and 85%, respectively. It is indicated with the increase of the window diameters, the acoustic resonances in the ADM increased. This improvement starts to be

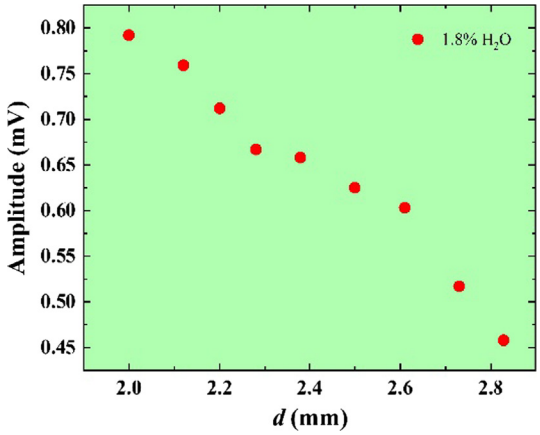

Fig. 4. The QEPAS signal amplitude as a function of ADM length *d*.

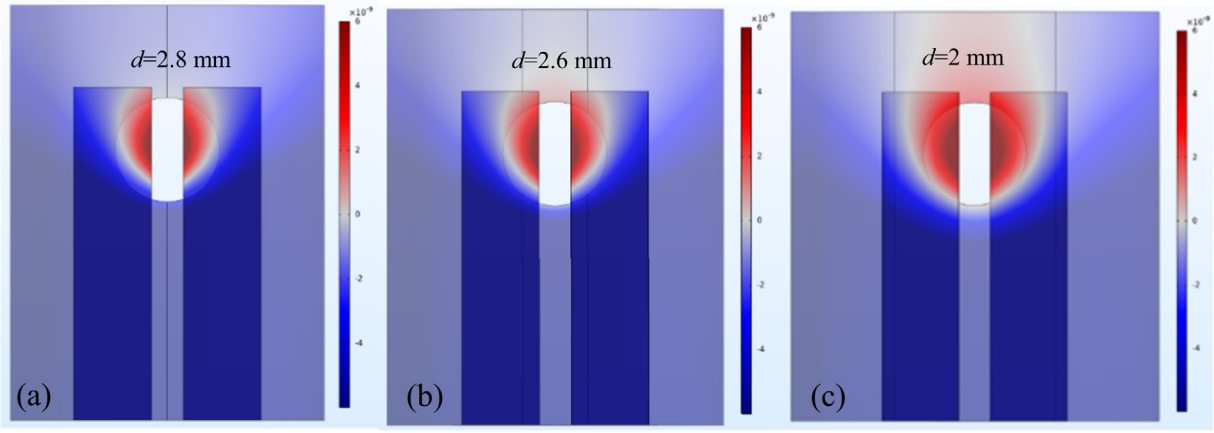

Fig. 3. Acoustic pressure in the ADM analyzed by FEM.

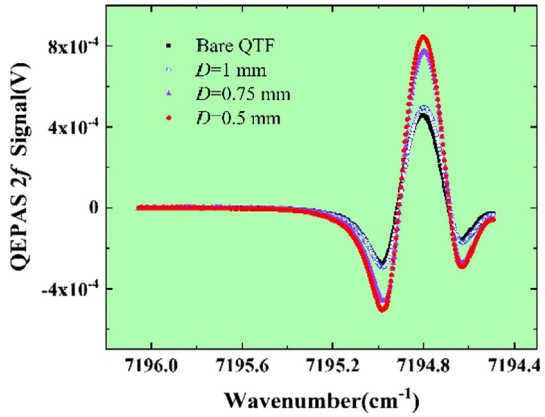

Fig. 5. QEPAS 2*f* signals obtained by four ADMs with different windows.

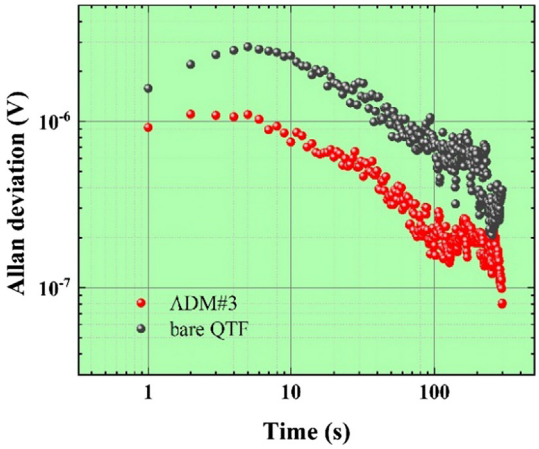

Fig. 6. The Allan variance of ADM#3 and bare QTF.

significant when the window diameter was $>$ 0.5 mm. With the laser wavelength tuned far away from the H_2O line, the 1σ noise ADM#1, #2, #3 and bare QTF were calculated to be 8.13 $\times$ 10^{-7} V, 9.06 $\times$ 10^{-7} V, 9.16 $\times$ 10^{-7} V, and 1.28 $\times$ 10^{-6} V respectively. The QTF itself is a detector for multi-wavelength radiation from micro waves to terahertz waves, as a result, the QTF is sensitive to the electromagnetic waves in the environments. When an ADM made of stainless steel was employed to cover the QTF, 1σ noise of the ADM decreased by 36.5%, from 1.28 $\times$ 10^{-6} V to 8.13 $\times$ 10^{-7} V. The reduce in 1σ noise can be attributed the suppression of electromagnetic waves and environmental noise. With the window diameter increasing from 0.5 mm to 1 mm, the 1σ noise increased by 12.6%. Nevertheless, the ADM#3 with D = 1 mm and d = 2 mm obtained a detection signal to noise ratio (SNR) of 926, when detecting 1.8% H_2O. The SNR was improved by 159%, compared to a bare QTF.

5. Long-term stability evaluation

In order to evaluate the long-term stability of the QEPAS sensor, an Allan variance of ADM#3 and bare QTF were performed. The laser wavelength was tuned to 7196.06 cm^{-1}, away from the H_2O absorption line located at 7194.8 cm^{-1}. As shown in Fig. 6., with the integration time of $\sim$ 100 s, the deviation of ADM#3 and bare QTF decreased by 85% and 73%, respectively. Both the ADM#3 and bare QTF showed a stable time of $\sim$ 300 s. With an integration time of 300 s, the 1σ deviation of ADM#3 reached $<$ 1 $\times$ 10^{-7} V, corresponding to a detection SNR of 8653 and a 2 ppm detection limit for H_2O.

6. Conclusion

An ultra-compact acoustic detection module (ADM) was developed for trace gas detection based on QEPAS. A novel gas enclosure was designed to confine the photoacoustic waves and excite the acoustic azimuthal and radial modes in QEPAS. Finite element modelling (FEM) method was performed to analyze the acoustic pressure distribution in the ADM. The length and window diameter of the ADM, which are related to the acoustic azimuthal and radial modes are experimentally optimized to enhance the sensor performance. The results obtained by experiment coincides well with the FEM analysis. With an ADM length of 2 mm and the window diameter of 1 mm, the ADM improved the detection SNR by 159%. Allan variance shows that long-term stability of the ADM and a bare QTF are comparable, however, the noise of the ultra-compact ADM was lower. With an integration time of 300 s, the developed QEPAS ADM achieved a detection limit of $\sim$ 2 ppm for H_2O, by utilizing a weak absorption line of 3.07 $\times$ 10^{-21} cm/mol and a low laser power of $\sim$ 5 mW. This detection sensitivity can be improved by choosing a strong H_2O absorption line and using a high power light source. The dimension comparison of current QEPAS ADMs was listed in Table 2. The developed QEPAS ADM was only $\sim$ 56.5 mm^3 (0.05 mL) and $\sim$ 0.15 g, which is outstanding in the laser spectroscopic gas sensors.

The volume of the developed ADM can be further decreased by using of a micro QTF [34]. The estimated ADM volume based on a micro QTF can be $<$ 5 mm^3. The gas enclosure-induced acoustic confinement can also be applied to the custom tuning forks, making the QEPAS ADM based on custom tuning fork more compact. The ultra-compact structure will significantly benefit the portability of the gas sensor, especially for the application on minimum unmanned aerial vehicles (UAVs) or unmanned surface vehicle (USVs).

Declaration of Competing Interest

No conflict of interest exits in the submission of this manuscript, and the manuscript is approved by all authors for publication.

Acknowledgements

The authors thank the Prof. Lei Dong and Prof. Hongpeng Wu of Shanxi University for the support in the experiment and discussing of results.

Funding

This work is supported by the National Natural Science Foundation of China (61675092, 61601404, 61705086), Natural Science

Table 1
Performance of QEPAS ADM with different window diameters. The 1σ noise was calculated with the laser wavelength centred away from the H_2O absorption line. F: frequency; SNR: signal to noise ratio.

ADM	*D* (mm)	*d* (mm)	F (Hz)	Signal (V)	Signal Gain	1σ Noise (V)	SNR	SNR Gain
#1	0.5	2	32755.5	4.95 $\times$ 10^{-4}	8%	8.13 $\times$ 10^{-7}	608	70%
#2	0.75	2	32756.9	7.92 $\times$ 10^{-4}	73%	9.06 $\times$ 10^{-7}	874	145%
#3	1	2	32758.8	8.48 $\times$ 10^{-4}	85%	9.16 $\times$ 10^{-7}	926	159%
Bare QTF	\	\	32757.4	4.57 $\times$ 10^{-4}	0	1.28 $\times$ 10^{-6}	357	0

Table 2
Comparison of several QEPAS ADM. *D*: diameter; *L*: length; *W*: width; *H*: height.

Shape	Material	Dimension (mm)	Volume (mm^3)	Reference
Cylinder	Steel	22 × 20.6 (*D* × *L*)	8186.6	[33]
Cuboid	Steel	25 × 25 × 15 (*L* × *W* × *H*)	9375	[9]
Cuboid	Steel	57 × 57 × 35 (*L* × *W* × *H*)	113,715	[28]
Cuboid	\	20 × 12.7 × 8.5(*L* × *W* × *H*)	2159	[23]
Cuboid	Polymer	29 × 15 (*L* × *W*)	\	[29]
Cylinder	Steel	3 × 8 (*D* × *L*)	56.5	This work

Foundation of Guangdong Province (2020B151502070, 2016A030313079, 2016A030311019, 2017A030313375, 2019A1515011380), Special Funds for Major Science and Technology Projects of Guangdong Province (2019B010138004, 2017A010102006, 2015B010125007), Project of Guangzhou Industry Leading Talents (CXLJTD-201607), and Planned Science & Technology Project of Guangzhou (201707010396, 2016B010111003), Joint fund of pre-research for equipment, Ministry of Education of China (6141A02022124), Aeronautical Science Foundation of China (201708W4001 ,201808W4001); Foundation for Distinguished Young Talents in Higher Education of Guangdong (2018KQNCX009, 2018KQNCX279), the Fundamental Research Funds for the Central Universities (21619402,11618413), State Key Laboratory of Applied Optics (SKLAO-201914). Frank Tittel acknowledges the financial support from the US National Science Foundation (NSF) ERC MIRTHE award, a NSF NeTS Large "ASTRO" award (No. R3H685) and a grant C-0586 from the Welch Foundation.

Appendix A. Supplementary material

Supplementary data to this article can be found online at https://doi.org/10.1016/j.infrared.2020.103278.

References

[1] H. Wu, X. Yin, L. Dong, Z. Jia, J. Zhang, F. Liu, W. Ma, L. Zhang, W. Yin, L. Xiao, S. Jia, F.K. Tittel, Ppb-level nitric oxide photoacoustic sensor based on a mid-IR quantum cascade laser operating at 52 °C, Sens. Actuat. B-Chem. 290 (2019) 426–433.
[2] Z. Bozóki, A. Szabó, Á. Mohácsi, G. Szabó, A fully opened photoacoustic resonator based system for fast response gas concentration measurements, Sens. Actuat. B-Chem. 147 (2010) 206–212.
[3] P. Patimisco, G. Scamarcio, F.K. Tittel, V. Spagnolo, Quartz-enhanced photoacoustic spectroscopy: a review, Sens.-Basel 14 (2014) 6165–6206.
[4] A. Berrou, M. Raybaut, A. Godard, M. Lefebvre, High-resolution photoacoustic and direct absorption spectroscopy of main greenhouse gases by use of a pulsed entangled cavity doubly resonant OPO, Appl. Phys. B-Lasers O. 98 (2010) 217.
[5] H. Wu, L. Dong, X. Yin, A. Sampaolo, P. Patimisco, W. Ma, L. Zhang, W. Yin, L. Xiao, V. Spagnolo, S. Jia, Atmospheric CH_4 measurement near a landfill using an ICL-based QEPAS sensor with VT relaxation self-calibration, Sens.. Actuat. B-Chem. 297 (2019) 126753.
[6] Y. Ma, Y. Tong, Y. He, X. Jin, F.K. Tittel, Compact and sensitive mid-infrared all-fiber quartz-enhanced photoacoustic spectroscopy sensor for carbon monoxide detection, Opt. Exp. 27 (2019) 9302–9312.
[7] A.A. Kosterev, Y.A. Bakhirkin, R.F. Curl, F.K. Tittel, Quartz-enhanced photoacoustic spectroscopy, Opt. Lett. 27 (2002) 1902–1904.
[8] J. Hayden, B. Baumgartner, J.P. Waclawek, B. Lendl, Mid-infrared sensing of CO at saturated absorption conditions using intracavity quartz-enhanced photoacoustic spectroscopy, Appl. Phys. B 125 (2019) 159.
[9] L. Dong, V. Spagnolo, R. Lewicki, F.K. Tittel, Ppb-level detection of nitric oxide using an external cavity quantum cascade laser based QEPAS sensor, Opt. Exp. 19 (2011) 24037–24045.
[10] A.A. Kosterev, F.K. Tittel, D.V. Serebryakov, A.L. Malinovsky, I.V. Morozov, Applications of quartz tuning forks in spectroscopic gas sensing, Rev. Sci. Instrum. 76 (2005) 043105.
[11] K. Liu, J. Li, L. Wang, T. Tan, W. Zhang, X. Gao, W. Chen, F.K. Tittel, Trace gas sensor based on quartz tuning fork enhanced laser photoacoustic spectroscopy, Appl. Phys. B-Lasers O. 94 (2009) 527–533.
[12] H. Yi, W. Chen, S. Sun, K. Liu, T. Tan, X. Gao, T-shape microresonator-based high sensitivity quartz-enhanced photoacoustic spectroscopy sensor, Opt. Exp. 20 (2012) 9187–9196.
[13] Z. Wang, Q. Wang, J.Y.L. Ching, J.C.Y. Wu, G. Zhang, W. Ren, A portable low-power QEPAS-based CO_2 isotope sensor using a fiber-coupled interband cascade laser, Sens. Actuat. B-Chem. 246 (2017) 710–715.
[14] V. Spagnolo, P. Patimisco, S. Borri, G. Scamarcio, B.E. Bernacki, J. Kriesel, Mid-infrared fiber-coupled QCL-QEPAS sensor, Appl. Phys. B-Lasers O. 112 (2013) 25–33.
[15] G. Wysocki, A.A. Kosterev, F.K. Tittel, Influence of molecular relaxation dynamics on quartz-enhanced photoacoustic detection of CO_2 at $\lambda = 2$ μm, Appl. Phys. B-Lasers O. 85 (2006) 301–306.
[16] P. Patimisco, A. Sampaolo, L. Dong, F.K. Tittel, V. Spagnolo, Recent advances in quartz enhanced photoacoustic sensing, Appl. Phys. Rev. 5 (2018) 011106.
[17] S. Li, L. Dong, H. Wu, A. Sampaolo, P. Patimisco, V. Spagnolo, F.K. Tittel, Ppb-level quartz-enhanced photoacoustic detection of carbon monoxide exploiting a surface grooved tuning fork, Anal. Chem. 91 (2019) 5834–5840.
[18] Y. Ma, Y. He, P. Patimisco, A. Sampaolo, S. Qiao, X. Yu, F.K. Tittel, V. Spagnolo, Ultra-high sensitive trace gas detection based on light-induced thermoelastic spectroscopy and a custom quartz tuning fork, Appl. Phys. Lett. 116 (2020) 011103.
[19] Y. He, Y. Ma, Y. Tong, X. Yu, F.K. Tittel, Ultra-high sensitive light-induced thermoelastic spectroscopy sensor with a high Q-factor quartz tuning fork and a multipass cell, Opt. Lett. 44 (2019) 1904–1907.
[20] Y. Ma, Y. He, Y. Tong, X. Yu, F.K. Tittel, Quartz-tuning-fork enhanced photothermal spectroscopy for ultra-high sensitive trace gas detection, Opt. Exp. 26 (2018) 32103–32110.
[21] T. Wei, H. Wu, L. Dong, Acoustic Detection Module Design of a Quartz-Enhanced Photoacoustic Sensor, Sensors-Basel 19 (2019) 1093.
[22] A.A. Kosterev, F.K. Tittel, Ammonia detection by use of quartz-enhanced photoacoustic spectrophone with a near-IR telecommunication diode laser, Appl. Opt. 43 (2004) 6213–6217.
[23] L. Dong, A.A. Kosterev, D. Thomazy, F.K. Tittel, QEPAS spectrophones: design, optimization, and performance, Appl. Phys. B 100 (2010) 627–635.
[24] P. Patimisco, A. Sampaolo, L. Dong, M. Giglio, G. Scamarcio, F.K. Tittel, V. Spagnolo, Analysis of the electro-elastic properties of custom quartz tuning forks for optoacoustic gas sensing, Sens. Actuat. B-Chem. 227 (2016) 539–546.
[25] M. Giglio, A. Elefante, P. Patimisco, A. Sampaolo, F. Sgobba, H. Rossmadl, V. Mackowiak, H. Wu, F.K. Tittel, L. Dong, V. Spagnolo, Quartz-enhanced photoacoustic sensor for ethylene detection implementing optimized custom tuning fork-based spectrophone, Opt. Exp. 27 (2019) 4271–4280.
[26] F.K. Tittel, A. Sampaolo, P. Patimisco, L. Dong, A. Geras, T. Starecki, V. Spagnolo, Analysis of overtone flexural modes operation in quartz-enhanced photoacoustic spectroscopy, Opt. Exp. 24 (2016) 257598.
[27] P. Patimisco, A. Sampaolo, H. Zheng, L. Dong, F.K. Tittel, V. Spagnolo, Quartz–enhanced photoacoustic spectrophones exploiting custom tuning forks: a review, Adv. Phys. X 2 (2017) 169–187.
[28] H. Wu, A. Sampaolo, L. Dong, P. Patimisco, X. Liu, H. Zheng, X. Yin, W. Ma, L. Zhang, W. Yin, V. Spagnolo, S. Jia, F.K. Tittel, Quartz enhanced photoacoustic $_H2S$ gas sensor based on a fiber-amplifier source and a custom tuning fork with large prong spacing, Appl. Phys. Lett. 107 (2015) 111104.
[29] X. Yang, Y. Xiao, Y. Ma, Y. He, F.K. Tittel, A Miniaturized QEPAS trace gas sensor with a 3D-printed acoustic detection module, Sensors-Basel 17 (2017) 1750.
[30] V. Spagnolo, A.A. Kosterev, L. Dong, R. Lewicki, F.K. Tittel, NO trace gas sensor based on quartz-enhanced photoacoustic spectroscopy and external cavity quantum cascade laser, Appl. Phys. B-Lasers O. 100 (2010) 125–130.
[31] H. Wu, L. Dong, H. Zheng, Y. Yu, W. Ma, L. Zhang, W. Yin, L. Xiao, S. Jia, F.K. Tittel, Beat frequency quartz-enhanced photoacoustic spectroscopy for fast and calibration-free continuous trace-gas monitoring, Nat. Commun. 8 (2017) 15331.
[32] The HITRAN database can be available online by Http://hitran.org.
[33] H. Zheng, L. Dong, X. Yin, X. Liu, H. Wu, L. Zhang, W. Ma, W. Yin, S. Jia, Ppb-level QEPAS NO_2 sensor by use of electrical modulation cancellation method with a high power blue LED, Sens. Actuat. B-Chem. 208 (2015) 173–179.
[34] H. Lin, Z. Huang, R. Kan, H. Zheng, Y. Liu, B. Liu, L. Dong, W. Zhu, J. Tang, J. Yu, Z. Chen, F.K. Tittel, Application of Micro Quartz Tuning Fork in trace gas sensing by use of quartz-enhanced photoacoustic spectroscopy, Sensors-Basel 19 (2019) 5240.